Development 138, 1573-1582 (2011) doi:10.1242/dev.060467

Interaction between *alk1* and blood flow in the development of arteriovenous malformations

Paola Corti[1], Sarah Young[1], Chia-Yuan Chen[2], Michael J. Patrick[3], Elizabeth R. Rochon[1], Kerem Pekkan[2] and Beth L. Roman[1,*]

SUMMARY

Arteriovenous malformations (AVMs) are fragile direct connections between arteries and veins that arise during times of active angiogenesis. To understand the etiology of AVMs and the role of blood flow in their development, we analyzed AVM development in zebrafish embryos harboring a mutation in *activin receptor-like kinase I* (*alk1*), which encodes a TGFβ family type I receptor implicated in the human vascular disorder hereditary hemorrhagic telangiectasia type 2 (HHT2). Our analyses demonstrate that increases in arterial caliber, which stem in part from increased cell number and in part from decreased cell density, precede AVM development, and that AVMs represent enlargement and stabilization of normally transient arteriovenous connections. Whereas initial increases in endothelial cell number are independent of blood flow, later increases, as well as AVMs, are dependent on flow. Furthermore, we demonstrate that *alk1* expression requires blood flow, and despite normal levels of shear stress, some flow-responsive genes are dysregulated in *alk1* mutant arterial endothelial cells. Taken together, our results suggest that Alk1 plays a role in transducing hemodynamic forces into a biochemical signal required to limit nascent vessel caliber, and support a novel two-step model for HHT-associated AVM development in which pathological arterial enlargement and consequent altered blood flow precipitate a flow-dependent adaptive response involving retention of normally transient arteriovenous connections, thereby generating AVMs.

KEY WORDS: Arteriovenous malformation, Alk1/Acvrl1, Hereditary hemorrhagic telangiectasia, Zebrafish

INTRODUCTION

Arteriovenous malformations (AVMs) are abnormal direct connections between arteries and veins that manifest as tortuous, rupture-prone vessels through which gas and nutrient exchange is impaired. Although the majority of AVMs are asymptomatic, clinical outcomes can range from focal hypoxia to stroke, depending on lesion size, location and stability (Letteboer et al., 2006). Generally, AVMs are thought to form during active angiogenesis. However, their pathogenesis is poorly understood.

Although most AVMs are sporadic, a small percentage are attributed to mutations in genes involved in TGFβ superfamily signaling. Collectively, this family of autosomal dominant diseases is known as hereditary hemorrhagic telangiectasia (HHT). HHT1 is caused by mutations in the gene encoding endoglin (*ENG*), a type III accessory receptor; HHT2 is caused by mutations in the gene encoding activin receptor like kinase 1 (*ALK1* or *ACVRL1*), a type I receptor; and HHT-juvenile polyposis syndrome is caused by mutations in *SMAD4* (McAllister et al., 1994; Johnson et al., 1996; Gallione et al., 2004). Although HHT1 and HHT2 are fully penetrant disorders, they exhibit variable expressivity, age of onset and lesion location. Variability is not allele based and is hypothesized to stem from genetic or environmental modifiers that have yet to be uncovered (Bourdeau et al., 2000).

[1]Department of Biological Sciences, University of Pittsburgh, Pittsburgh, PA 15260, USA. [2]Department of Biomedical and Mechanical Engineering, Carnegie Mellon University, Pittsburgh, PA 15210, USA. [3]Molecular Biosensor and Imaging Center, Carnegie Mellon University, Pittsburgh, PA 15213, USA.

*Author for correspondence (romanb@pitt.edu)

Accepted 25 January 2011

In TGFβ family signaling (for a review, see Ross and Hill, 2008), ligand dimers bind to a complex of two type II and two type I receptors, each of which is a transmembrane serine/threonine kinase. Ligand binding, which can be facilitated by type III receptors, stimulates the type II receptor to phosphorylate the type I receptor, which then phosphorylates receptor-specific R-Smads. Phosphorylated R-Smads bind to the common partner SMAD, SMAD4, translocate to the nucleus and transcriptionally regulate target genes. Although BMP9, BMP10, TGFβ1 and TGFβ3 can each bind ALK1 and stimulate phosphorylation of SMAD1 and SMAD5 within particular experimental contexts (Lux et al., 1999; Oh et al., 2000; Brown et al., 2005; David et al., 2007a; Scharpfenecker et al., 2007), the physiologically relevant ALK1 ligand required to prevent AVMs is unknown.

There is considerable discrepancy in the literature concerning the role of ALK1 within endothelial cells: although some studies suggest a role in angiogenic activation, characterized by growth of new vessels from existing vessels, others suggest a role in resolution, characterized by stabilization of new vessels. In support of a role in activation, constitutively active ALK1 induces *inhibitor of differentiation-1* (*ID1*), which maintains cells in a proliferative state, and increases migration and cell number in some cultured endothelial cells (Goumans et al., 2002). In support of a role in resolution, $Alk1^{-/-}$ mice exhibit enlarged major vessels, increased expression of endothelial mitogens and failed vascular smooth muscle recruitment (Oh et al., 2000; Urness et al., 2000). Furthermore, treatment with BMP9, a high-affinity ALK1 ligand that circulates at physiologically relevant concentrations, inhibits proliferation and migration in cultured endothelial cells and inhibits angiogenesis in multiple in vivo assays (Brown et al., 2005; David et al., 2007b; Scharpfenecker et al., 2007; David et al., 2008). Thus, the preponderance of evidence suggests a role for ALK1 in

resolution, although the possibility of alternative ALK1 ligands or downstream effectors mediating different effects in endothelial cells cannot be discounted.

Although the function of ALK1 within endothelial cells is not clear, it is undoubtedly crucial in development of normal arteriovenous connections. Global or endothelial cell-specific deletion of *Alk1* in embryonic mice results in lethal AVMs, whereas global deletion of *Alk1* during adulthood results in AVMs in active angiogenic vessels (Oh et al., 2000; Urness et al., 2000; Park et al., 2008; Park et al., 2009). We have previously reported that, in zebrafish embryos, *alk1* (*acvr1l* – Zebrafish Information Network) is expressed exclusively in arteries proximal to the heart, and that *alk1* mutations cause embryonic AVMs that develop at a predictable time, in a predictable location (Roman et al., 2002). The accessibility and optical clarity of zebrafish embryos afford us the opportunity to watch AVMs develop in real time, and to probe the molecular and cellular mis-steps and environmental factors that precipitate these lethal abnormalities. Our results demonstrate that blood flow triggers *alk1* expression in nascent arteries exposed to high hemodynamic forces, and that Alk1 functions to limit vessel caliber. In the absence of *alk1*, Alk1-dependent arteries enlarge, and downstream vessels adapt to consequent increases in flow by retaining normally transient arteriovenous drainage connections that enlarge into AVMs. As AVM development in zebrafish *alk1* mutants is fully dependent on blood flow, we suggest that AVMs in individuals with HHT are not fully genetically determined but represent normal adaptive responses to altered blood flow.

MATERIALS AND METHODS

Zebrafish lines and maintenance

Zebrafish (*Danio rerio*) were maintained according to standard protocols (Westerfield, 1995). When appropriate, embryo medium was supplemented with 0.003% phenylthiourea (PTU) (Sigma, St Louis, MO, USA) at 24 hours post-fertilization (hpf) to prevent melanin formation (Kimmel et al., 1995). Mutant lines *alk1*^{y6}, *chrna1*^{b107}, *cxcr4a*^{um20}, *edn1*^{tf216b}, *gata1a*^{m651} and *tnnt2a*^{tc300b} have been previously described (Sepich et al., 1998; Miller et al., 2000; Lyons et al., 2002; Roman et al., 2002; Sehnert et al., 2002; Siekmann et al., 2009). Genotyping assays for *alk1*^{y6} and *cxcr4a*^{um20} have been described previously (Roman et al., 2002; Siekmann et al., 2009). *edn1*^{tf216b} genotype was assayed by dCAPS (Neff et al., 1998) using FP1 5′-CCAACTTTGAGGTCCCGTGTGATG-3′, RP1 5′-CAAAAGTAG-ACGCACTCGTTA-3′ (53°C annealing) and DdeI (cuts mutant allele). Transgenic lines *Tg(fli1a:nEGFP)*^{y7}, *Tg(kdrl:GFP)*^{la116} and *Tg(gata1:dsRed)*^{sd2} have been previously described (Roman et al., 2002; Traver et al., 2003; Choi et al., 2007). The endothelial membrane-localized *fli1a.ep:mRFP-F* transgene was generated by Gateway cloning (Invitrogen, Carlsbad, CA, USA), recombining *pTolfli1a.epDest* (Villefranc et al., 2007) with monomeric red fluorescent protein (mRFP) appended with a 3′ CAAX (prenylation) site. This construct was injected along with *transposase* mRNA (Kawakami et al., 2004) into one-cell embryos to generate *Tg(fli1a.ep:mRFP-F)*^{pt505}.

Morpholinos and drug exposures

Morpholino-modified antisense oligonucleotides (GeneTools, Philomath, OR, USA) were injected into embryos at the one- to four-cell stage. Translation blocking *tnnt2a* morpholino (4 ng) (5′-CATGTTTCG-TCTGATCTGACACGCA-3′) (Sehnert et al., 2002) eliminated heartbeat in nearly all injected embryos. The *alk1* morpholino (5′-ATCGGTTT-CACTCACCAACACACTC-3′) targeted the exon 6/intron 6 splice donor site and produced AVMs in 90-95% of injected embryos at 2.5 ng. Splice-blocking efficacy was validated at 36 hpf by RT-PCR, using forward primer 5′-TGCTACGTACCTGCTATTCCTGG-3′ (exon 4) and reverse primer 5′-GGTGCCCACTCTCGGATTG-3′ (exon 9), followed by shotgun cloning (pCRII-TOPO, Invitrogen) and sequencing (see Fig. S1 in the supplementary material). Translation blocking *klf2a* morpholino (10 ng) (5′-GGACCTGTCCAGTTCATCCTTCCAC-3′) generated the previously published aortic arch 5/6 pulsation phenotype (Nicoli et al., 2010) in 44% of embryos (15/34) and consistently upregulated *klf2a* expression (see Fig. S2 in the supplementary material). To stop heartbeat, embryos were incubated in 800 μg/ml tricaine in 30% Danieau/0.003% PTU.

In situ hybridization

Whole-mount in situ hybridization was performed as previously described (Roman et al., 2002). Plasmids used to generate riboprobes are described in Table S1 in the supplementary material. Bright-field images were captured using an MVX-10 MacroView macro zoom microscope equipped with an MV PLAPO 1×/0.25 NA objective, 2× magnification changer and DP71 camera with DP controller software version 3.1 (Olympus America, Center Valley, PA, USA). Embryos derived from *alk1*$^{+/-}$, *cxcr4a*$^{+/-}$ and *edn1*$^{+/-}$ incrosses were genotyped subsequent to imaging and phenotypic analysis. Images were compiled using Adobe Photoshop CS2 version 9.0.2 (Adobe Systems, San Jose, CA, USA).

Confocal imaging and microangiography

Zebrafish embryos were anesthetized with 160 μg/ml tricaine (Sigma) or fixed in 4% paraformaldehyde and inserted into 500 μm agarose troughs made in a bed of 2% agarose mounted on a glass slide. *z*-series of frame-averaged optical sections were acquired with a FluoView500 or FluoView1000 laser-scanning confocal microscope (Olympus) outfitted with an LUMPLFL 40×/0.8 or UMPLFL 20×/0.5 NA water immersion objective, or with a Bio-Rad Radiance 2000 laser-scanning confocal microscope (Carl Zeiss Microimaging, Thornwood, NJ, USA) outfitted with a Fluor 40×/0.8 water immersion objective. Projections were generated using ImageJ version 1.43 (NIH, Bethesda, MD, USA), and endothelial cells counted as previously described (Roman et al., 2002). To eliminate differences in endothelial cell number due to ongoing development, cell counting was performed on images of precisely staged, paraformaldehyde-fixed embryos. Comparison of cell counts in embryos prior to and after fixation (4% paraformaldehyde, 2 hours at room temperature, followed by storage in PBS, 4°C for 1 week) revealed comparable numbers (n=5; see Fig. S3 in the supplementary material). Images were compiled using Photoshop. For microangiography, Qtracker 655 non-targeted quantum dots (Invitrogen) diluted in distilled water to 1 μM were microinjected into the common cardinal vein. Vessel volumes were measured from confocal angiograms using Imaris version 6.3 (Bitplane, St Paul, MN, USA), and endothelial cell density calculated by dividing the number of endothelial cell nuclei by vessel volume. Embryos from *alk1*$^{+/-}$, *alk1*$^{+/-}$;*cxcr4a*$^{+/-}$ and *alk1*$^{+/-}$;*edn1*$^{+/-}$ incrosses were genotyped subsequent to imaging and phenotypic analysis.

High speed particle image velocimetry and wall shear stress calculation

To measure wall shear stress (WSS), blood flow in embryos from an *alk1*$^{+/-}$;*chrna1*$^{+/-}$;*Tg(kdrl:GFP)*^{la116};*Tg(gata1:dsRed)*^{sd2} incross was imaged at 32-36 hpf using high-speed confocal microscopy. Only immobile embryos homozygous for the *chrna1*^{b107} mutation were imaged, circumventing the need for anesthesia that might affect heart rate. Imaging was performed on a Leica TCS SP5 confocal microscope (Leica Microsystems, Wetzlar, Germany) with Argon (488 nm) and HeNe (543 nm) lasers, a phase-matched bidirectional resonant scanner (16,000 Hz), and 20×/0.70 NA oil objective. Spectral detection windows (Hamamatsu R6357 photomultiplier tube) were 495-536 nm for GFP and 555-640 nm for dsRed. The region of interest was 256×64 pixels, resulting in a frame acquisition rate of 175 fps. Four-thousand frames were recorded per data set, encompassing ~20 cardiac cycles. The pulsatile velocity distribution of red blood cell flow in the distal first aortic arch was calculated using time-lapsed images following a previously validated particle image velocimetry (PIV) measurement protocol (Patrick et al., 2010). Briefly, a fast Fourier transform cyclic algorithm was used to process PIV time series images, and velocity vectors were calculated using multi-pass cross-correlation algorithms (DaVis 7.2 PIV software, LaVision, Ypsilanti, MI, USA). WSS (t) was calculated as t=m·du/dr, where m is blood viscosity [assumed to be 5×10^{-3} N·s·m^{-2} (Hove et al., 2003)] and du/dr is the streamwise velocity gradient along the diameter of the arch vessel. Instantaneous streamwise

velocity was extracted from a 50×30 pixel ROI within a two-dimensional time lapse PIV velocity map. The streamwise velocity component was integrated along the vessel cross-section, providing the instantaneous average blood velocity. Very low Womersley numbers (0.03) and rigid cells with embryonic nuclei (i.e. existence of Newtonian flow) justified the assumption of a quasi-steady parabolic velocity profile (Wang et al., 2009). Conservation of mass, as well as the no-slip boundary condition at the vessel walls, allowed estimation of instantaneous WSS values. For each embryo, three cardiac cycles were averaged to account for cycle to cycle variations.

Statistical analysis

Vessel volume, wall shear stress and endothelial cell number data were analyzed by Student's *t*-test. Gene expression data were analyzed by Fisher's exact test. Significance was set at $P \leq 0.05$.

RESULTS

Blood flow modifies endothelial cell number in the basal communicating artery and posterior communicating segments in *alk1* mutants

In wild-type zebrafish embryos at 48 hpf (Fig. 1A), blood flows from the heart to the midbrain and hindbrain via the first aortic arch, internal carotid artery and its caudal division (CaDI), basal communicating artery (BCA), posterior communicating segments (PCS) and basilar artery (BA). From the PCS and BA, which lie just ventral to the midbrain and hindbrain, blood perfuses the brain via capillary-like central arteries (not shown), then drains to the sequentially arranged lateral head veins, the primordial midbrain channel (PMBC) and primordial hindbrain channel (PHBC). By contrast, 48 hpf *alk1* mutant embryos (Fig. 1A) exhibit dramatically enlarged high-flow cranial AVMs that shunt blood from the BCA or BA directly to the venous PMBC or PHBC, bypassing the central arteries (Roman et al., 2002). We have previously reported that artery enlargement in 48 hpf *alk1* mutants is due in part to increased endothelial cell number, with the 'triangle' of vessels comprising the BCA and PCS containing approximately twice the number of endothelial cells as in wild-type siblings (Roman et al., 2002). To determine the age of onset of this phenotype, we examined endothelial cell number in the BCA/PCS in wild-type and *alk1* mutant *Tg(fli1a:nEGFP)*^{y7} embryos, beginning at 26 hpf, the time point at which angiogenic sprouts from the CaDI first contribute to the nascent BCA (see Fig. 3B, 26 hpf). Between 26 and 30 hpf, no differences were observed in endothelial cell number in the developing BCA/PCS (Fig. 1B,C; compare *alk1*$^{-/-}$ with wild type). By contrast, by 32 hpf, a small, but statistically significant, 1.2-fold increase in endothelial cell number was observed in *alk1* mutants (Fig. 1C). The fold change in endothelial cell number increased in magnitude over time, reaching a 1.8-fold increase by 48 hpf (Fig. 1B,C).

We reasoned that increases in cell number in *alk1* mutants might represent an adaptive response to altered blood flow. Blood vessels are exposed to biomechanical forces imparted by flow, namely circumferential strain, which stretches the vessel wall perpendicular to the direction of flow, and shear stress, a frictional force that acts on endothelial cells parallel to the direction of flow (for a review, see Lehoux and Tedgui, 2003). Vessels strive to normalize these forces, and do so by modulating vessel wall thickness and lumen diameter in response to circumferential strain and shear stress, respectively. To determine whether blood flow is necessary for increases in endothelial cell number in *alk1* mutants, we compared the BCA/PCS in *alk1* mutants with normal heartbeat to *alk1* mutants with noncontractile hearts, effected by injection of a *troponin-t2a* (*tnnt2a*) morpholino. The oxygen needs of zebrafish embryos can be met by diffusion rather than by circulation so *tnnt2a* morphants are not hypoxic (Jacob et al., 2002). As expected, vessels were collapsed in the absence of perfusion, but vessel architecture was otherwise relatively normal up to 40 hpf, though the PCSs appeared shortened by 48 hpf (Fig. 1B, *tnnt2a* MO). Between 32 and 40 hpf, BCA/PCS endothelial cell numbers in *alk1*$^{-/-}$, *alk1*$^{-/-}$*;tnnt2a MO* and *tnnt2a MO* were indistinguishable from one another and significantly increased compared with wild type, suggesting that these increases in cell number in *alk1* mutants are not flow dependent, and that the lack of flow itself can trigger a response similar to loss of *alk1* (Fig. 1B,C). By contrast, the large increase in endothelial cell number in *alk1* mutants arising between 40 and 48 hpf was completely abrogated in the absence of flow (Fig. 1B,C). To confirm this latter result using an alternative approach, we allowed embryos to develop normal heartbeat and circulation, then stopped heartbeat with tricaine exposure between 42 and 50 hpf. Whereas this treatment had no effect on wild-type embryos, it significantly decreased BCA/PCS endothelial cell number in *alk1* mutants (Fig. 1D). These results demonstrate that early increases in cell number in *alk1* mutants occur irrespective of flow status, whereas later increases require blood flow.

AVMs in *alk1* mutants represent retention of normally transient arteriovenous connections in response to increased blood flow

In addition to increases in cell number, *alk1* mutants develop cranial AVMs with 100% penetrance. We employed confocal microscopy to elucidate the origin of these AVMs, which connect either the BCA to the PMBC or the BA to the PHBC. In wild-type embryos, blood flowing from the CaDI into the newly formed BCA drains to the PMBC via a pair of bilateral PMBC-derived vessels until ~32 hpf (Fig. 2A). As the downstream PCSs and BA begin to carry flow, these drainage connections are no longer required and ultimately regress. By contrast, in *alk1* mutants (Fig. 2A), one or both of these connections may enlarge and persist, accounting for the BCA/PMBC AVMs. The more posterior BA/PHBC AVMs arise in *alk1* mutants in a similar manner. In wild-type embryos, multiple angiogenic sprouts from the PHBCs appear around 27 hpf, coursing beneath the hindbrain toward the midline to not only generate the BA but also to serve as early drainage (Fig. 2A; see Movie 1 in the supplementary material). Again, these conduits regress in wild-type embryos but may enlarge and persist in *alk1* mutants, accounting for the BA/PHBC AVMs (Fig. 2A). Note that the size and therefore dominance of any given shunt may change over time (see Fig. S4 in the supplementary material), but at least one normally transient arteriovenous connection is retained in the absence of *alk1*.

To determine whether blood flow plays a role in AVM development in *alk1* mutants, we analyzed vessel morphology in *alk1* mutants subjected to altered flow conditions (Fig. 2B). Importantly, *alk1* mutants lacking heartbeat do not develop AVMs (0/11 *alk1*$^{-/-}$*;tnnt2a MO*), whereas *alk1* mutants that have heartbeat and plasma flow but no erythrocytes invariably develop AVMs (7/7 *alk1*$^{-/-}$*;gata1a*$^{-/-}$). These results demonstrate that AVMs in *alk1* mutants are not simply genetically determined, and that blood flow, but not erythrocyte/endothelial cell interactions, is required to precipitate AVM development.

Alk1 expression requires blood flow

Based on the observation that BCA/PCS endothelial cell number in *tnnt2a* morphants is similar to *alk1* mutants (Fig. 1C), we reasoned that *alk1* expression may be regulated by blood flow. To test this

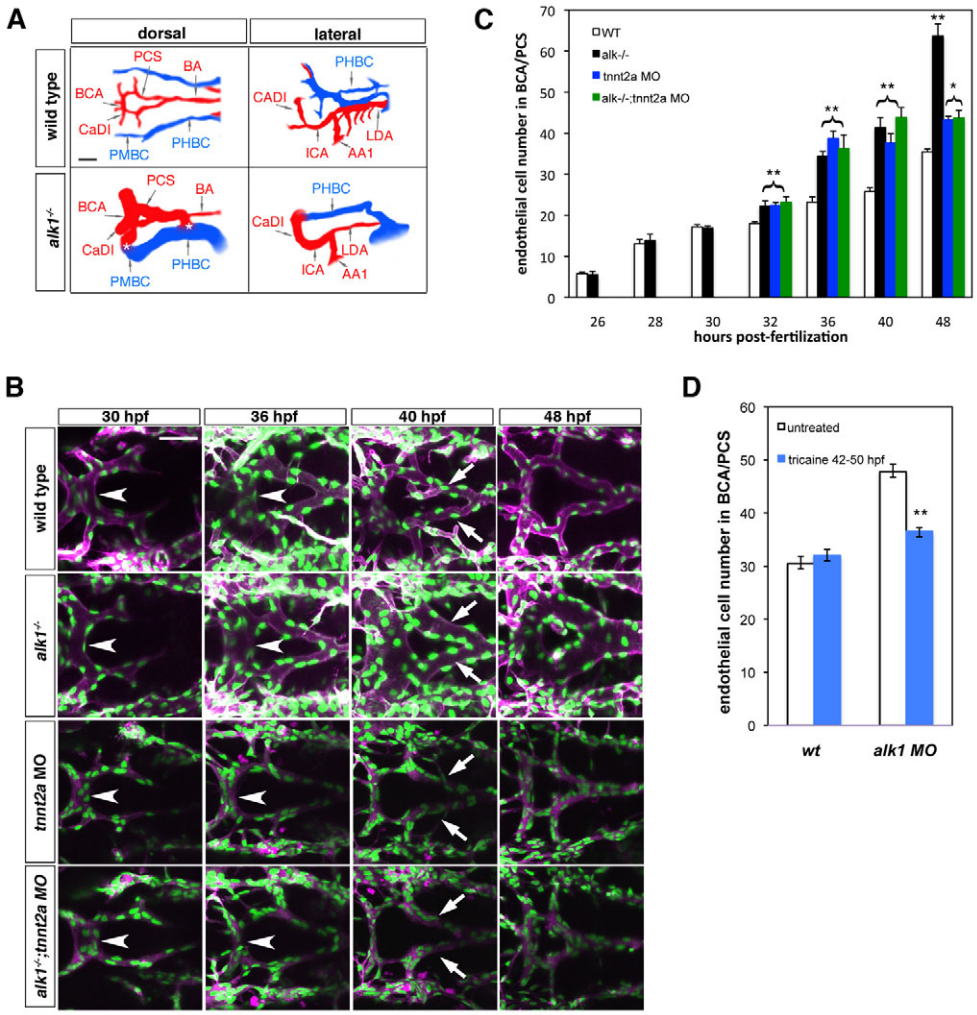

Fig. 1. Blood flow modifies endothelial cell number in *alk1* mutants. (**A**) Wiring diagrams of perfused head vessels in 48 hpf wild-type and *alk1*$^{-/-}$ embryos, derived from two-dimensional confocal projections of *Tg(gata1:dsRed)*^{sd2} embryos. Arteries are red; veins are blue. *alk1* mutants exhibit enlarged arteries and AVMs (*) between the BCA/PMBC and/or BA/PHBC. Vessels represented in wild-type embryos but not *alk1*$^{-/-}$ embryos are present but not patent in mutants. AA1, first aortic arch; BA, basilar artery; BCA, basal communicating artery; CaDI, caudal division of internal carotid artery; ICA, internal carotid artery; LDA, lateral dorsal aorta; PCS, posterior communicating segments; PHBC, primordial hindbrain channel; PMBC, primordial midbrain channel. Scale bar: 50 μm. (**B**) Development of the BCA/PCSs in wild type (row 1), *alk1*$^{-/-}$ (row 2), *tnnt2a* morphants (MO) (row 3) and *alk1*$^{-/-}$*;tnnt2a* MO (row 4). Images are two-dimensional confocal projections of live *Tg(fli1a:nEGFP)*^{y7}*;Tg(fli1a.ep:mRFP-F)*^{pt505} embryos, dorsal views, anterior leftwards. Endothelial cell nuclei are green; endothelial cell membranes are magenta. In *alk1*$^{-/-}$, the BCA (arrowhead) is enlarged by 36 hpf, and the PCSs (arrows) by 40 hpf. BCA/PCS morphology is relatively normal in *tnnt2* MO and *alk1*$^{-/-}$*;tnnt2* MO, although vessels are collapsed. Scale bar: 50 μm. (**C**) Quantification of endothelial cell number from confocal micrographs of fixed *Tg(fli1a:nEGFP)*^{y7} embryos. *alk1*$^{-/-}$ with (black bars) or without (green bars) blood flow show similar increases in endothelial cell number compared with wild-type siblings (white bars) between 32-40 hpf, although the pronounced increase between 40 and 48 hpf observed in *alk1*$^{-/-}$ depends on blood flow. Cell number in *tnnt2a* MO (blue bars) is not different from cell number in *alk1*$^{-/-}$*;tnnt2a* MO, suggesting that lack of flow phenocopies *alk1* mutants in terms of endothelial cell number. Data represent mean±s.e.m. (*n*=3-13 independent samples) and were analyzed by Student's *t*-test. *P<0.01; **P<0.001. (**D**) Quantification of endothelial cell number from confocal micrographs of 50 hpf wild-type or *alk1* MO Tg*(fli1a:nEGFP)*^{y7} embryos treated with tricaine between 42 and 50 hpf. The increase in endothelial cell number observed at 40-48 hpf in *alk1* morphants is reduced by stopping blood flow. Data represent mean±s.e.m. (*n*=4-8 independent samples) and were analyzed by Student's *t*-test. **P<0.001.

hypothesis, we assessed the spatiotemporal pattern of *alk1* expression and found a striking correlation with flow onset. Expression of *alk1* is first detectable around 26 hpf in the perfused arteries most proximal to the heart: the first aortic arches (AA1) and the caudalward lateral dorsal aortae (LDA) (Fig. 3A,B). The cranialward internal carotid arteries (ICAs) and CaDIs are visible at 26 hpf; however, these vessels neither carry blood flow nor are *alk1* positive at this time (Fig. 3A,B; lateral, frontal). Perfusion of the internal carotid arteries and CaDIs is apparent by 28 hpf, at which time the internal carotids express *alk1* along their entire length, whereas the CaDIs express *alk1* only at their most proximal ends (Fig. 3A,B). By 30 hpf, robust circulation through the CaDIs correlates with *alk1* expression along their entire length, and the now patent BCA also expresses *alk1* (Fig. 3A,B). Expression of *alk1* in these arteries persists until at least 48 hpf, though peak levels occur around 40 hpf (P.C., unpublished). Notably, the PCSs and BA carry blood flow by 32-36 hpf (Fig. 3B). However, neither of

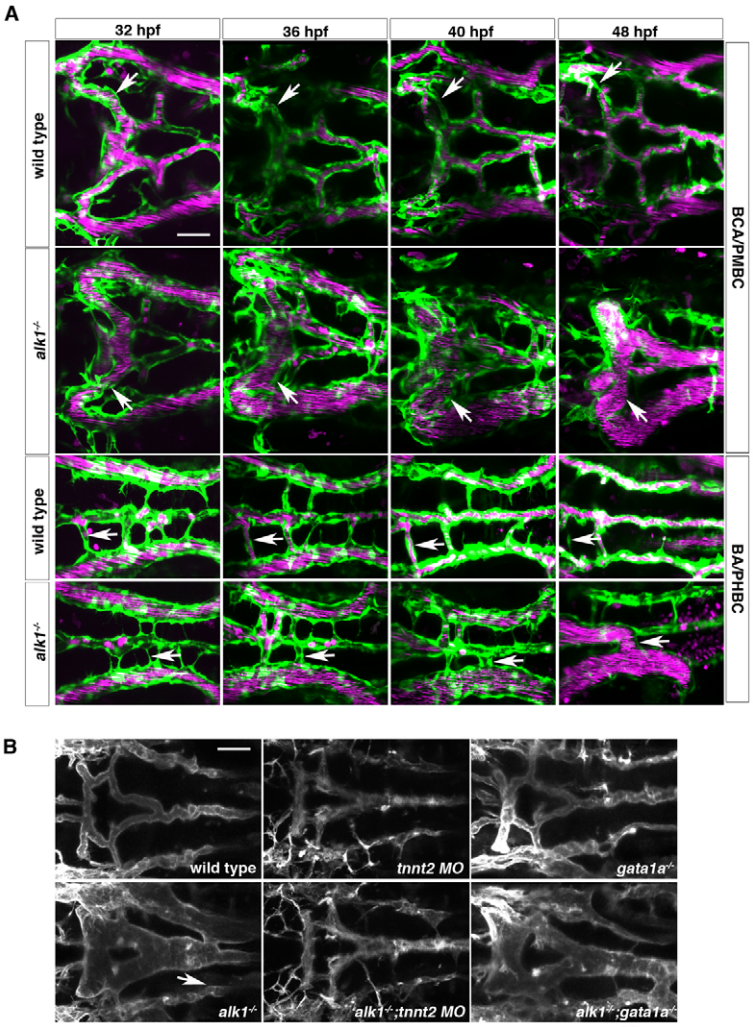

Fig. 2. Retention of normally transient arteriovenous connections in *alk1* mutants is flow dependent. (**A**) In wild-type embryos (row 1), transient connections between the basal communicating artery (BCA) and primordial midbrain channel (PMBC) carry blood at 32 hpf but regress by 48 hpf (arrows). In *alk1* mutants (row two), one or both of these bilateral connections may be retained, forming a BCA-to-PMBC AVM (arrows). More posteriorly, lumenized connections drain the basilar artery (BA) to the primordial hindbrain channel (PHBC) in wild-type embryos at early times, but almost all regress by 48 hpf (row 3, arrows). In *alk1* mutants, one or more of these connections may be retained, forming a BA-to-PHBC AVM (row 4, arrows). Images are two-dimensional confocal projections of *Tg(kdrl:GFP)*^{la116}*; Tg(gata1:dsRed)*^{sd2} embryos, dorsal views, anterior leftwards. Endothelial cells are green; erythrocytes are magenta. (**B**) AVMs (arrows) are detectable in 48 hpf *alk1*$^{-/-}$ embryos and in *alk1*$^{-/-}$*;gata1a*$^{-/-}$ embryos (which lack erythrocytes), but not in *alk1*$^{-/-}$*;tnnt2* MO (which lack blood flow). Images are two-dimensional confocal projections of *Tg(fli1a.ep:mRFP-F)*^{pt505} embryos, dorsal views, anterior leftwards. Scale bars: 50 μm.

these vessels nor any other cranial arteries or veins express detectable levels of *alk1* at this time (Fig. 3A; see wiring diagrams, with *alk1*-positive vessels in pink). Taken together, these data demonstrate that the arteries most proximal to the heart, which experience the highest levels of circumferential strain and shear stress, express *alk1* concomitant with blood flow.

To further investigate the relationship between blood flow and *alk1* expression, we examined *alk1* expression in *tnnt2a* mutants. In the absence of blood flow, *alk1* expression was undetectable by in situ hybridization (Fig. 3C; see Table S2 in the supplementary material). Furthermore, abrogation of heartbeat by treatment with tricaine severely downregulated *alk1* expression (Fig. 3C; see Table S2 in the supplementary material). By contrast, *alk1* expression was not altered in *gata1a* mutants (Fig. 3C; see Table S2 in the supplementary material), which have normal heartbeat and plasma flow but lack erythrocytes. Expression of another endothelial cell-specific gene, *cadherin 5*, was not influenced by flow status (Fig. 3C; see Table S2 in the supplementary material), demonstrating that changes in *alk1* expression were not due to gross changes in vessel morphology or global changes in the endothelial cell transcriptional program. These data demonstrate that *alk1* expression requires blood flow, and that sensitivity to flow is imparted either by mechanical forces or circulating factors, but not by erythrocyte/endothelial cell interactions.

Loss of *alk1* dysregulates expression of some blood flow-responsive genes

Although the above data clearly demonstrate that blood flow is required for *alk1* expression, they cannot distinguish between a role for mechanical forces versus circulating factors in *alk1* induction. Both circumferential strain and shear stress regulate expression of many genes in endothelial cells, allowing these biomechanical signals to be transduced to biochemical signals that facilitate adaptation to changes in blood flow (Lehoux and Tedgui, 2003). If *alk1* expression is induced by mechanical forces, we reasoned that *alk1* might lie in a mechanotransduction pathway either upstream or downstream of known mechanoresponsive genes. Therefore, we examined *alk1* mutants (32-40 hpf) for expression of three genes known to be responsive to cyclic strain and/or shear stress, and examined *alk1* expression in embryos in which these mechanoresponsive genes were disrupted.

KLF2 encodes a transcription factor that is upregulated by shear stress and integrates several shear stress-responsive pathways (Dekker et al., 2005; Parmar et al., 2006). As expected, endothelial expression of the zebrafish *KLF2* ortholog, *klf2a*, was severely downregulated in *tnnt2a* mutants and in wild-type embryos exposed to tricaine (Fig. 4A; see Table S2 in the supplementary material), confirming previous findings (Parmar et al., 2006). However, *klf2a* expression was not different in *alk1* mutants

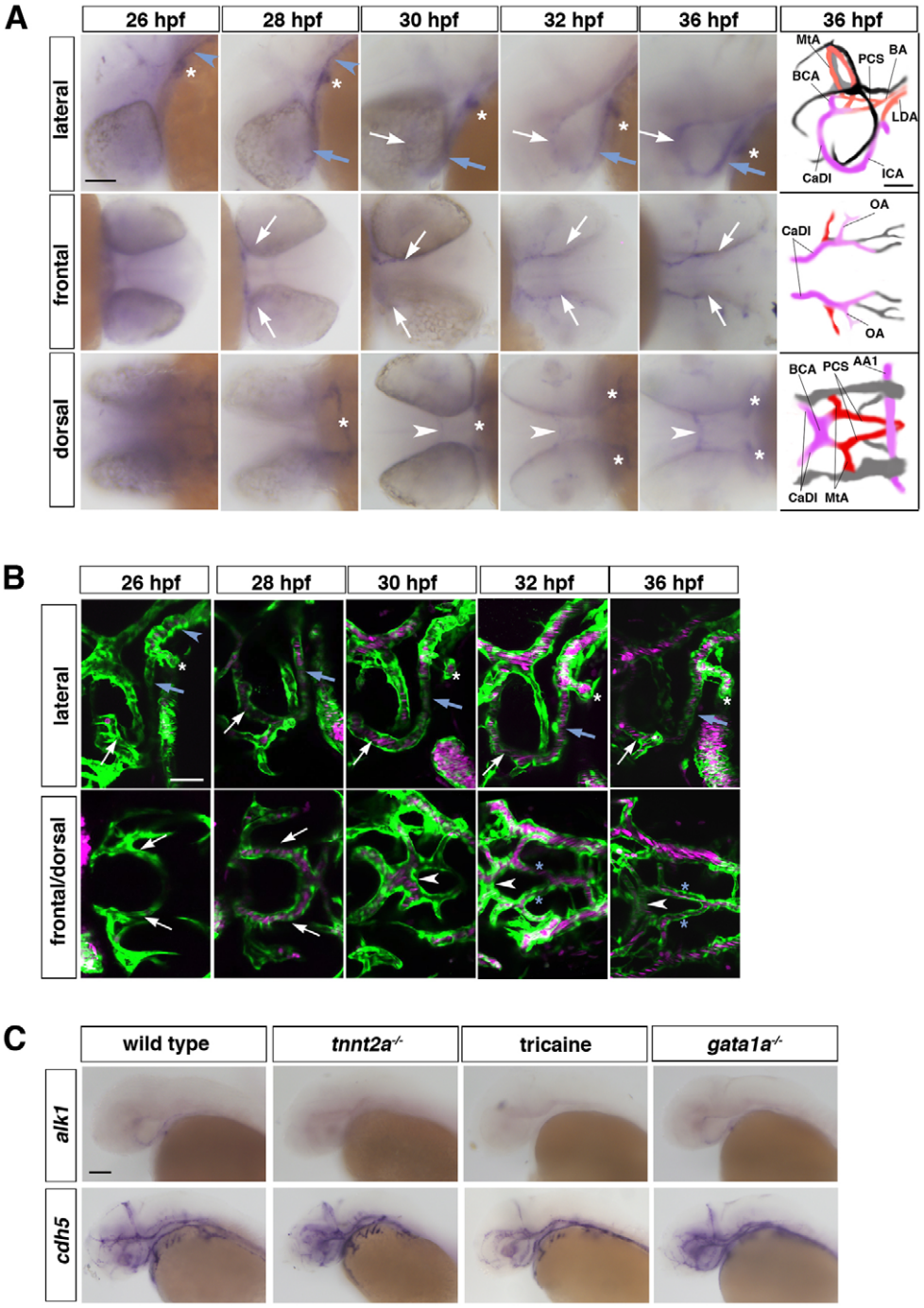

Fig. 3. *alk1* expression requires blood flow. (**A**) Spatiotemporal pattern of *alk1* mRNA expression assayed by whole-mount in situ hybridization. Expression is detected in the first aortic arch (AA1, white asterisk), lateral dorsal aorta (LDA; blue arrowhead) and internal carotid artery (ICA, blue arrow) at 26-28 hpf, then in the caudal division of the internal carotid artery (CaDI, white arrow) and basal communicating artery (BCA, white arrowhead) by 28-30 hpf. Tracings in the far right column represent all vessels expressing *cdh5* at 36 hpf, with *alk1*-positive arteries in pink, *alk1*-negative arteries in red and veins in black or gray. BA, basilar artery; LDA, lateral dorsal aortae; MtA, metencephalic artery; OA, optic artery; PCS, posterior communicating segments. Lateral and dorsal views, anterior leftwards. Frontal view, anterior rightwards. Scale bar: 50 μm. (**B**) Onset of blood flow correlates with *alk1* expression. At 26 hpf, blood flows caudally through AA1 (asterisk) and the LDA (blue arrowhead). The cranialward ICA (blue arrow) and CaDI (white arrow) carry flow by 28 hpf; the BCA (white arrowhead) by 30 hpf; and the PCSs (blue asterisks) by 32 hpf. Images are two-dimensional confocal projections of *chrna1*$^{-/-}$ (paralyzed), *Tg(kdrl:GFP)*^{la116}*;Tg(gata1:dsRed)*^{sd2} embryos. Endothelial cells are green, erythrocytes are magenta. Lateral and dorsal views (row 2, columns 3-5), anterior leftwards. Frontal view (row 2, columns 1-2), anterior rightwards. Scale bar: 50 μm. (**C**) Whole-mount in situ hybridization demonstrates that *alk1* is downregulated in the absence of blood flow (*tnnt2a*$^{-/-}$ or tricaine treatment, 32-40 hpf) but is not affected by the absence of erythrocytes (*gata1a*$^{-/-}$). *cdh5* expression is unchanged under all conditions. All embryos are at 36 hpf except tricaine treated, which are at 40 hpf. Lateral views, anterior leftwards. Scale bar: 100 μm.

compared with wild-type embryos (Fig. 4A; see Table S2 in the supplementary material). Endothelin 1 (*EDN1*) encodes a vasoconstrictive peptide that is transcriptionally downregulated by laminar shear stress and upregulated by cyclic strain (Sharefkin et al., 1991; Wang et al., 1993; Dekker et al., 2005). Vascular *edn1* expression, which was detectable only in the first aortic arch, internal carotid artery, CaDI and lateral dorsal aortae in wild-type embryos, was nearly undetectable in *tnnt2a* mutants, tricaine-treated embryos and *alk1* mutants (Fig. 4A; see Table S2 in the supplementary material). Notably, these arteries are *alk1* positive (Fig. 3A), and the cranial *edn1*-positive arteries are enlarged in *alk1* mutants (Roman et al., 2002). Finally, *CXCR4* encodes a promigratory chemokine receptor that is transcriptionally downregulated by laminar shear stress (Melchionna et al., 2005). Vascular expression of the zebrafish *CXCR4* ortholog *cxcr4a* was upregulated in arteries in *tnnt2a* mutants, tricaine-treated embryos and *alk1* mutants (Fig. 4A; see Table S2 in the supplementary material). As changes in *edn1* and *cxcr4a* in *alk1* mutants correlate with changes in embryos lacking blood flow, these results suggest that *alk1* may be important in flow-based induction and repression, respectively, of these mechanosensitive genes. Epistasis experiments placed *klf2a* in a pathway independent from *alk1*, *cxcr4a* and *edn1*. None of these genes was dysregulated in *klf2a* morphants (see Fig. S2 and Table S2 in the supplementary

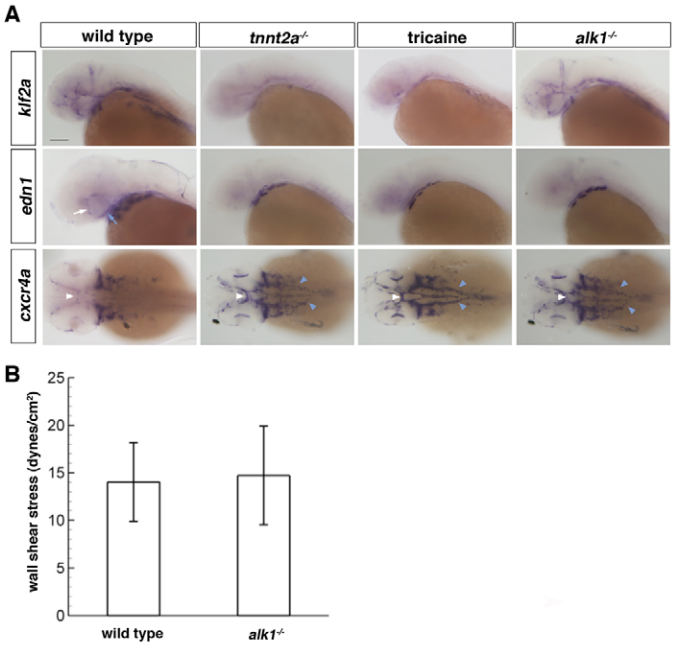

Fig. 4. Loss of *alk1* dysregulates expression of flow-responsive genes but does not alter shear stress. (**A**) Whole-mount in situ hybridization using *klf2a*, *edn1* and *cxcr4a* riboprobes. Vascular *klf2a* expression is strongly downregulated in the absence of blood flow (*tnnt2a*$^{-/-}$ or tricaine treatment, 32-40 hpf) but is unaltered in *alk1*$^{-/-}$ embryos. By contrast, vascular *edn1* expression is downregulated and *cxcr4a* expression is upregulated both in the absence of flow and in *alk1* mutants. Changes in expression are primarily in *alk1*-positive arteries: ICA (blue arrow) and CaDI (white arrow), BCA (white arrowhead) and LDA (blue arrowhead), as well as AA1 (not shown). Lateral expression of both *edn1* and *cxcr4a* is in the pharyngeal arches and is unchanged in all conditions. All embryos are 36 hpf except tricaine treated, which are 40 hpf. *klf2a* and *edn1*, lateral views, anterior leftwards. *cxcr4a*, dorsal view, anterior leftwards. Scale bar: 100 μm. (**B**) Blood flow in the distal region of AA1 was imaged in *chrna1*$^{-/-}$ (paralyzed) *Tg(kdrl:GFP)*^{la116}*;Tg(gata1:dsRed)*^{sd2} *alk1* mutant embryos and wild-type/heterozygous siblings at 32-36 hpf by high-speed confocal microscopy, and particle image velocimetry used to calculate wall shear stress. Results represent mean±s.d., *n*=8 wild type and *n*=5 *alk1* mutants. Differences were not significant according to Student's *t*-test.

material), nor was *klf2a* dysregulated in *alk1*, *edn1* or *cxcr4a* mutants (see Table S2 in the supplementary material). Furthermore, neither *edn1* nor *cxcr4a* was dysregulated in *cxcr4a* or *edn1* mutants, respectively, suggesting that these two genes do not lie in a linear pathway downstream of *alk1* (see Table S2 in the supplementary material).

Although the above data might suggest that *alk1* lies upstream of *edn1* and *cxcr4a* in a mechanotransduction pathway, observed changes in gene expression could reflect molecular readout of changes in hemodynamic forces resulting from enlargement of *alk1* mutant vessels. To determine whether shear stress is altered in *alk1* mutants, we used high-speed confocal micro-particle image velocimetry (Patrick et al., 2010) to generate averaged velocity profiles and calculate wall shear stress (WSS) in *alk1* mutants and their wild-type siblings. We measured WSS in the distal first aortic arch, which expresses *alk1* and, in *alk1* mutants, enlarges and exhibits changes in shear-responsive gene expression (see Fig. S5 in the supplementary material). Results demonstrate that WSS in 32-36 hpf *alk1* mutants is not different from phenotypically wild-type siblings, averaging ~14-15 dyne/cm^2 in both groups (Fig. 4B). Taken together with the lack of effect of *alk1* loss on *klf2a* expression, these results argue that changes in shear stress cannot account for observed changes in *edn1* and *cxcr4a* expression.

Vasodilation contributes to increased arterial caliber in *alk1* mutants

Given that vascular *edn1* expression was localized primarily in *alk1*-positive vessels that enlarge in *alk1* mutants and *edn1* was lost in *alk1* mutant arteries, we hypothesized that *edn1* loss might result in vasodilation, contributing to increased vessel caliber and AVM development. In support of this hypothesis, endothelial cell density was decreased in *alk1* mutant BCAs (Fig. 5A). However, *edn1*$^{-/-}$*; alk1*$^{+/+}$ (*n*=13) and *edn1*$^{-/-}$*;alk1*$^{+/-}$ (*n*=3) embryos displayed normal cranial vessels (Fig. 5B), and we observed no genetic interaction between *alk1* and *edn1* when graded doses of *alk1* morpholino were injected into embryos from an *edn1*$^{+/-}$ incross (S.Y., unpublished). We also examined the role of upregulation of *cxcr4a*, which not only plays a role in endothelial cell migration but has also been linked to vasodilatory nitric oxide production (You et al., 2006), in AVM development. All *cxcr4a*$^{-/-}$*;alk1*$^{-/-}$ embryos developed AVMs (*n*=12/12), though the PCSs were typically smaller and/or incompletely formed in both *cxcr4a*$^{-/-}$*;alk1*$^{-/-}$ and *cxcr4a*$^{-/-}$ (*n*=3) embryos (Fig. 5B). In summary, although vasodilation contributes to increased vessel caliber in *alk1* mutants, *edn1* loss is not sufficient, nor is *cxcr4a* upregulation necessary, to induce the *alk1* mutant phenotype.

DISCUSSION

Loss of *alk1* function in zebrafish embryos results in lethal AVMs that develop in a precise spatiotemporal pattern, making this accessible model an invaluable tool for uncovering the molecular and cellular errors that lead to HHT-associated AVM development. In this study, we demonstrate that increases in endothelial cell number in *alk1*-positive arteries precede development of high flow shunts in *alk1* mutants, and that AVMs represent aberrant retention of transient venous-derived conduits that normally serve to drain the developing arterial system. Initial increases in endothelial cell number in *alk1* mutants are independent of blood flow, suggesting a primary defect directly attributable to loss of *alk1*. However, the contributions of increased proliferation, decreased apoptosis and altered endothelial cell migration to vessel enlargement in zebrafish *alk1* mutants remain to be determined. Overexpression of constitutively active *ALK1* or treatment with BMP9 inhibits endothelial cell proliferation in certain cultured endothelial cells (Lamouille et al., 2002; Scharpfenecker et al., 2007; David et al., 2008) and inducible loss of *Eng* in the mouse neonatal retina increases endothelial cell proliferation (Mahmoud et al., 2010), suggesting that increased proliferation may play a role in this phenotype. On the other hand, in a mouse *Notch4*-induced AVM model, increased vessel caliber precedes AVM development, as in zebrafish *alk1* mutants, but increased cell number stems not from increased proliferation but potentially from decreased angiogenic sprouting (Carlson et al., 2005).

Although initial increases in endothelial cell number in *alk1* mutant arteries occur irrespective of blood flow, later increases in cell number and AVMs require flow. These observations suggest a model for AVM development in *alk1* mutants in which the primary lesion, impaired resolution of nascent cranial arteries proximal to the heart, leads to increased vessel caliber and enhanced flow capacity. In the absence of blood flow, this lesion is self-limiting.

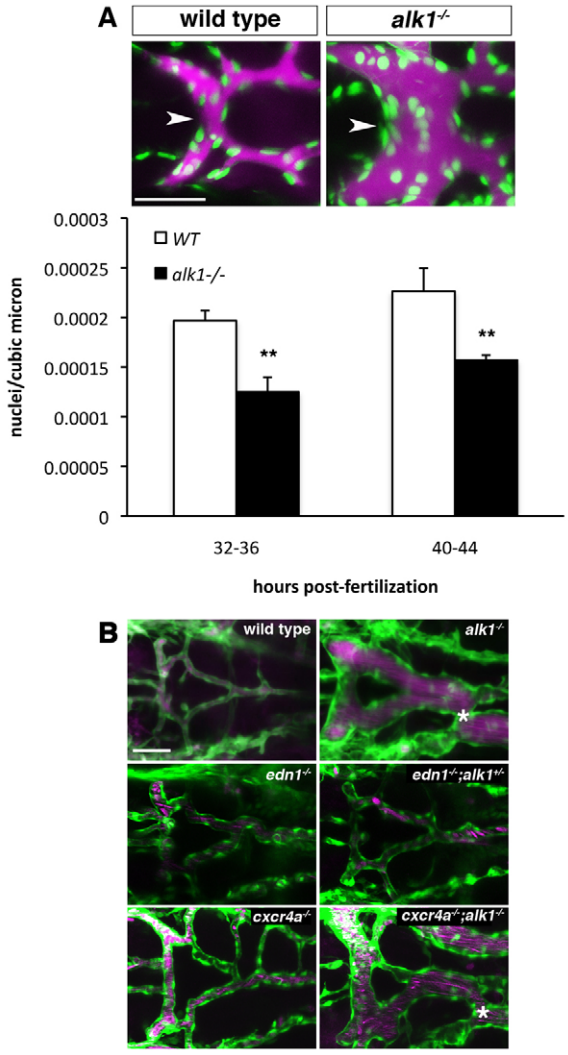

Fig. 5. Vasodilation contributes to increased vessel caliber in *alk1* mutants. (**A**) Qtracker 655 non-targeted quantum dots were injected into the common cardinal vein of wild-type and *alk1* mutant Tg*(fli1a:nEGFP)*^{y7} embryos. Images are two-dimensional confocal projections, dorsal views, anterior leftwards. Embryos aged 32-36 hpf are shown. Endothelial cell nuclei are green; quantum dots are magenta. Scale bar: 50 μm. Endothelial cell density in the BCA (white arrowhead) was calculated from these micrographs by dividing the number of nuclei by the vessel volume. Data represent mean±s.e.m. (*n*=5-7 independent samples) and were analyzed using Student's *t*-test, $^{**}P<0.001$. (**B**) Analysis of the contribution of *edn1* loss and *cxcr4a* upregulation to AVM development. AVM development in *alk1*$^{-/-}$ embryos (asterisk) is not phenocopied by *edn1*$^{-/-}$ embryos even in the presence of heterozygous levels of *alk1* (*edn1*$^{-/-}$;*alk*$^{+/-}$). *cxcr4a*$^{-/-}$ embryos do not exhibit AVMs, whereas *cxcr4a*$^{-/-}$;*alk1*$^{+/-}$ embryos invariably develop AVMs, demonstrating that *cxcr4a* upregulation is not necessary for AVM development in *alk1* mutants. Two-dimensional confocal projections of *Tg(fli1a:EGFP)*^{y1};*Tg(gata1:dsRed)*^{sd2} or *Tg(kdrl:GFP)*^{la116};*Tg(gata1:dsRed)*^{sd2} embryos. Endothelial cells are green; erythrocytes are magenta. Dorsal views, anterior leftwards. Scale bar: 50 μm.

However, the presence of flow stimulates further enlargement of these arteries, as well as downstream Alk1-independent arteries in an attempt to normalize hemodynamic forces. To drain this engorged arterial system, a variable complement of normally transient arteriovenous connections develop into large shunts or AVMs. Thus, we purport that AVMs in *alk1* mutants represent a normal adaptive response to increased blood flow. Strong support for this mechanism comes from data showing that embryonic vessels lacking smooth muscle cells adapt to increased shear stress by increasing lumen diameter (Taber et al., 2001) and from a mathematical model predicting AVM development stemming from a microshunt that lacks flow regulation (Quick et al., 2001). Furthermore, in *Alk1*$^{+/-}$ mice, vasodilation leading to increased tissue perfusion enhances cerebral capillary dysplasia during VEGF-induced angiogenesis, supporting the idea that the interaction between genetics and flow is crucial in HHT expressivity (Hao et al., 2008).

Although our *alk1* mutant zebrafish model strongly suggests that AVMs represent abnormal retention of transient arteriovenous connections in response to high blood flow, alternative mechanisms have been proposed. In *Eng*- and *Alk1*-null mice, the loss of the arterial marker *Ephrinb2* and thus the loss of arterial identity has been suggested to be the cause of AVMs (Urness et al., 2000; Sorensen et al., 2003). However, more recent data fail to demonstrate deficiencies in arteriovenous identity in an inducible *Eng*-null mouse (Mahmoud et al., 2010). We see no gain of venous identity, as assessed by *vegfr3* expression, in *alk1* mutant cranial arteries, but have been unable to investigate arterial identity because we have yet to identify an arterial marker, apart from *alk1*, that is clearly expressed in the cranial arteries affected by loss of *alk1* (B.L.R., unpublished).

Blood flow clearly plays a role not only in phenotype development in *alk1* mutants, but also in *alk1* expression, as *alk1* is not expressed in zebrafish embryos in the absence of blood flow. Although circumferential strain, shear stress or circulating factors may underlie this phenomenon, several pieces of evidence suggest a role for shear stress. For example, *Alk1* expression is upregulated in arteries presumed to be experiencing high shear stress in a mouse mesenteric artery ligation model (Seki et al., 2003), and shear stress induces *Alk1* expression in endothelial progenitor cells (Obi et al., 2009). Furthermore, because *alk1* loss affects arterial lumen caliber and not wall thickness, it seems more likely that Alk1 function is pertinent to the response to shear stress and not strain. Evidence against a role for shear stress in *alk1* expression, however, comes from the observation that *alk1* expression is normal in *gata1a* mutants, which have plasma flow but no erythrocytes and thus should have lower blood viscosity and shear stress. However, expression of other known shear stress-responsive genes, including *edn1*, *cxcr4a and klf2a*, is also unchanged in *gata1a* mutants (see Table S2 in the supplementary material).

The loss of expression of *alk1* in the absence of flow and the increase in cell number in *alk1* mutant arteries suggest that Alk1 functions in a flow-responsive pathway responsible for limiting nascent arterial caliber. In an attempt to define the molecular pathway downstream of Alk1, we examined expression of *edn1*, *cxcr4a* and *klf2a* in *alk1* mutants. Although both *EDN1* and *CXCR4* expression are downregulated in cultured human endothelial cells in response to shear stress (Sharefkin et al., 1991; Melchionna et al., 2005), we observed loss of *edn1* and induction of *cxcr4a* in *alk1* mutants. However, similar changes in gene expression were observed in *tnnt2a* morphants and tricaine-treated embryos, which experience no shear stress. These data suggest that, in vivo, shear stress (or the combination of shear stress and other flow-based factors) upregulates *edn1* and downregulates *cxcr4a*, and that *alk1* mutants mimic loss of flow in terms of *edn1* and *cxcr4a* expression. Although decreased levels of shear stress in

enlarged *alk1* mutants might explain these observations, we detected no deficit in shear stress in *alk1* mutant arteries that exhibit dysregulated gene expression, nor any effect on expression of the shear stress-responsive *klf2a*. These data, along with additional epistasis results (see Table S2 in the supplementary material), suggest that Alk1 may act upstream of *edn1* and *cxcr4a* in transducing shear forces in a pathway independent of *klf2a*. Although *KLF2* has been shown to regulate both *EDN1* and *CXCR4* in cultured human endothelial cells (Dekker et al., 2005; Uchida et al., 2009) the lack of effect of *klf2a* knockdown on these genes in zebrafish is not unanticipated given the lack of effect on expression of numerous *Klf2*-responsive genes, including *Edn1*, in *Klf2* null mice (Lee et al., 2006).

Although flow-dependent induction of *alk1* is necessary for stabilization of nascent arteries proximal to the heart, flow-dependent increases in cell number and development of AVMs in *alk1* mutants are clearly *alk1*-independent. It is tempting to speculate that both of these pathways are induced by shear stress, yet have opposite effects on vessel caliber. It remains to be determined whether differential pathway activation is determined by spatiotemporal patterns of gene expression, levels and/or types of shear stress (reversing versus unidirectional), alternative mechanical forces or circulating factors.

Our data demonstrate that, in addition to increased cell number, decreased endothelial cell density contributes to increased vessel caliber in *alk1* mutants. Given the coincidence of expression of *alk1* and *edn1*, and the loss of *edn1* in *alk1* mutants, it is logical to consider that loss of Edn1, a vasoconstrictive peptide, could lead to vasodilation and contribute to AVM development. A role for vasodilation in HHT1-associated AVM development has been previously suggested: in *ENG*-deficient endothelial cells, vasodilatory by-products of inefficient endothelial nitric oxide synthase activity are produced and prostaglandin synthesis is increased, resulting in enhanced vasodilation (Toporsian et al., 2005; Jerkic et al., 2006). Furthermore, downregulation of *EDN1* has been reported in human brain AVM samples (Rhoten et al., 1997). Although *edn1* mutants do not phenocopy *alk1* mutants in terms of vascular defects, there is considerable redundancy in Edn signaling in zebrafish, with six ligands that might induce vasoconstriction (Braasch et al., 2009). Furthermore, disruption of additional vasoactive pathways such as those described in *Eng*-deficient mice may be required in sum to elicit vasodilation. Ongoing studies are focused on investigating the role of Edn and other vasoactive pathways in vasodilation and AVM development in *alk1* mutants.

In conclusion, our data demonstrate that *alk1* expression requires blood flow and that Alk1 function in zebrafish embryonic endothelium is necessary to limit the caliber of nascent cranial arteries proximal to the heart. In the absence of *alk1*, these arteries deliver more blood volume to downstream vessels, which adapt by enlarging and retaining normally transient arteriovenous connections to drain this system. This two-step model suggests that HHT-associated AVM prevention and non-interventional treatment strategies could focus on preventing increases in cell number and vasodilation that contribute to arterial enlargement, and/or abrogating flow-induced AVM development. Identifying the signaling pathways and cellular behaviors involved in these distinct events will facilitate development of such strategies.

Acknowledgements

We are grateful to Zachary Kupchinsky for fish care; to Bhupendra Shravage and Katherine Somers for technical contributions; to Simon Watkins, Greg Gibson (University of Pittsburgh), Mohammed Islam and Deniz Kaya (Carnegie Mellon University) for access to confocal microscopes; to Nathan Lawson (University of Massachusetts Medical School), Chi-Bin Chien (University of Utah), Koichi Kawakami (National Institute of Genetics, Japan) and Brant Weinstein (NICHD) for plasmids; to Gage Crump (University of Southern California) for *edn1*^{tf216b} mutants; to Arndt Siekmann (Max-Planck Institute for Molecular Biomedicine) for *cxcr4a*^{um20} mutants; and to Christian Abnet (NCI) for statistical advice. This work was supported by NIH grant HL079108 (B.L.R.), by The Leslie Munzer Neurological Institute of Long Island (B.L.R.), by NSF CAREER 0954465 (K.P.), and by a Ri.Med Foundation Postdoctoral Fellowship (P.C.). Deposited in PMC for release after 12 months.

Competing interests statement

The authors declare no competing financial interests.

Supplementary material

Supplementary material for this article is available at
http://dev.biologists.org/lookup/suppl/doi:10.1242/dev.060467/-/DC1

References

Bourdeau, A., Faughnan, M. E. and Letarte, M. (2000). Endoglin-deficient mice, a unique model to study hereditary hemorrhagic telangiectasia. *Trends Cardiovasc. Med.* **10**, 279-285.

Braasch, I., Volff, J. N. and Schartl, M. (2009). The endothelin system: evolution of vertebrate-specific ligand-receptor interactions by three rounds of genome duplication. *Mol. Biol. Evol.* **26**, 783-799.

Brown, M. A., Zhao, Q., Baker, K. A., Naik, C., Chen, C., Pukac, L., Singh, M., Tsareva, T., Parice, Y., Mahoney, A. et al. (2005). Crystal structure of BMP-9 and functional interactions with pro-region and receptors. *J. Biol. Chem.* **280**, 25111-25118.

Carlson, T. R., Yan, Y., Wu, X., Lam, M. T., Tang, G. L., Beverly, L. J., Messina, L. M., Capobianco, A. J., Werb, Z. and Wang, R. (2005). Endothelial expression of constitutively active Notch4 elicits reversible arteriovenous malformations in adult mice. *Proc. Natl. Acad. Sci. USA* **102**, 9884-9889.

Choi, J., Dong, L., Ahn, J., Dao, D., Hammerschmidt, M. and Chen, J. N. (2007). FoxH1 negatively modulates flk1 gene expression and vascular formation in zebrafish. *Dev. Biol.* **304**, 735-744.

David, L., Mallet, C., Mazerbourg, S., Feige, J. J. and Bailly, S. (2007a). Identification of BMP9 and BMP10 as functional activators of the orphan activin receptor-like kinase 1 (ALK1) in endothelial cells. *Blood* **109**, 1953-1961.

David, L., Mallet, C., Vailhe, B., Lamouille, S., Feige, J. J. and Bailly, S. (2007b). Activin receptor-like kinase 1 inhibits human microvascular endothelial cell migration: potential roles for JNK and ERK. *J. Cell. Physiol.* **213**, 484-489.

David, L., Mallet, C., Keramidas, M., Lamande, N., Gasc, J. M., Dupuis-Girod, S., Plauchu, H., Feige, J. J. and Bailly, S. (2008). Bone morphogenetic protein-9 is a circulating vascular quiescence factor. *Circ. Res.* **102**, 914-922.

Dekker, R. J., van Thienen, J. V., Rohlena, J., de Jager, S. C., Elderkamp, Y. W., Seppen, J., de Vries, C. J., Biessen, E. A., van Berkel, T. J., Pannekoek, H. et al. (2005). Endothelial KLF2 links local arterial shear stress levels to the expression of vascular tone-regulating genes. *Am. J. Pathol.* **167**, 609-618.

Gallione, C. J., Repetto, G. M., Legius, E., Rustgi, A. K., Schelley, S. L., Tejpar, S., Mitchell, G., Drouin, E., Westermann, C. J. and Marchuk, D. A. (2004). A combined syndrome of juvenile polyposis and hereditary haemorrhagic telangiectasia associated with mutations in MADH4 (SMAD4). *Lancet* **363**, 852-859.

Goumans, M. J., Valdimarsdottir, G., Itoh, S., Rosendahl, A., Sideras, P. and ten Dijke, P. (2002). Balancing the activation state of the endothelium via two distinct TGF-beta type I receptors. *EMBO J.* **21**, 1743-1753.

Hao, Q., Su, H., Marchuk, D. A., Rola, R., Wang, Y., Liu, W., Young, W. L. and Yang, G. Y. (2008). Increased tissue perfusion promotes capillary dysplasia in the ALK1-deficient mouse brain following VEGF stimulation. *Am. J. Physiol. Heart Circ. Physiol.* **295**, H2250-H2256.

Hove, J. R., Koster, R. W., Forouhar, A. S., Acevedo-Bolton, G., Fraser, S. E. and Gharib, M. (2003). Intracardiac fluid forces are an essential epigenetic factor for embryonic cardiogenesis. *Nature* **421**, 172-177.

Jacob, E., Drexel, M., Schwerte, T. and Pelster, B. (2002). Influence of hypoxia and of hypoxemia on the development of cardiac activity in zebrafish larvae. *Am. J. Physiol. Regul. Integr. Comp. Physiol.* **283**, R911-R917.

Jerkic, M., Rivas-Elena, J. V., Santibanez, J. F., Prieto, M., Rodriguez-Barbero, A., Perez-Barriocanal, F., Pericacho, M., Arevalo, M., Vary, C. P., Letarte, M. et al. (2006). Endoglin regulates cyclooxygenase-2 expression and activity. *Circ. Res.* **99**, 248-256.

Johnson, D. W., Berg, J. N., Baldwin, M. A., Gallione, C. J., Marondel, I., Yoon, S. J., Stenzel, T. T., Speer, M., Pericak-Vance, M. A., Diamond, A. et al. (1996). Mutations in the activin receptor-like kinase 1 gene in hereditary haemorrhagic telangiectasia type 2. *Nat. Genet.* **13**, 189-195.

Kawakami, K., Takeda, H., Kawakami, N., Kobayashi, M., Matsuda, N. and Mishina, M. (2004). A transposon-mediated gene trap approach identifies developmentally regulated genes in zebrafish. *Dev. Cell* **7**, 133-144.

Kimmel, C. B., Ballard, W. W., Kimmel, S. R., Ullmann, B. and Schilling, T. F. (1995). Stages of embryonic development in the zebrafish. *Dev. Dyn.* **203**, 253-310.
Lamouille, S., Mallet, C., Feige, J. J. and Bailly, S. (2002). Activin receptor-like kinase 1 is implicated in the maturation phase of angiogenesis. *Blood* **100**, 4495-4501.
Lee, J. S., Yu, Q., Shin, J. T., Sebzda, E., Bertozzi, C., Chen, M., Mericko, P., Stadtfeld, M., Zhou, D., Cheng, L. et al. (2006). Klf2 is an essential regulator of vascular hemodynamic forces in vivo. *Dev. Cell* **11**, 845-857.
Lehoux, S. and Tedgui, A. (2003). Cellular mechanics and gene expression in blood vessels. *J. Biomech.* **36**, 631-643.
Letteboer, T. G., Mager, J. J., Snijder, R. J., Koeleman, B. P., Lindhout, D., Ploos van Amstel, J. K. and Westermann, C. J. (2006). Genotype-phenotype relationship in hereditary haemorrhagic telangiectasia. *J. Med. Genet.* **43**, 371-377.
Lux, A., Attisano, L. and Marchuk, D. A. (1999). Assignment of transforming growth factor β1 and β3 and a third new ligand to the type I receptor ALK-1. *J. Biol. Chem.* **274**, 9984-9992.
Lyons, S. E., Lawson, N. D., Lei, L., Bennett, P. E., Weinstein, B. M. and Liu, P. P. (2002). A nonsense mutation in zebrafish gata1 causes the bloodless phenotype in vlad tepes. *Proc. Natl. Acad. Sci. USA* **99**, 5454-5459.
Mahmoud, M., Allinson, K. R., Zhai, Z., Oakenfull, R., Ghandi, P., Adams, R. H., Fruttiger, M. and Arthur, H. M. (2010). Pathogenesis of arteriovenous malformations in the absence of endoglin. *Circ. Res.* **106**, 1425-1433.
McAllister, K. A., Grogg, K. M., Johnson, D. W., Gallione, C. J., Baldwin, M. A., Jackson, C. E., Helmbold, E. A., Markel, D. S., McKinnon, W. C., Murrell, J. et al. (1994). Endoglin, a TGF-β binding protein of endothelial cells, is the gene for hereditary haemorrhagic telangiectasia type 1. *Nat. Genet.* **8**, 345-351.
Melchionna, R., Porcelli, D., Mangoni, A., Carlini, D., Liuzzo, G., Spinetti, G., Antonini, A., Capogrossi, M. C. and Napolitano, M. (2005). Laminar shear stress inhibits CXCR4 expression on endothelial cells: functional consequences for atherogenesis. *FASEB J.* **19**, 629-631.
Miller, C. T., Schilling, T. F., Lee, K., Parker, J. and Kimmel, C. B. (2000). sucker encodes a zebrafish Endothelin-1 required for ventral pharyngeal arch development. *Development* **127**, 3815-3828.
Neff, M. M., Neff, J. D., Chory, J. and Pepper, A. E. (1998). dCAPS, a simple technique for the genetic analysis of single nucleotide polymorphisms: experimental applications in *Arabidopsis thaliana* genetics. *Plant J.* **14**, 387-392.
Nicoli, S., Standley, C., Walker, P., Hurlstone, A., Fogarty, K. E. and Lawson, N. D. (2010). MicroRNA-mediated integration of haemodynamics and Vegf signalling during angiogenesis. *Nature* **464**, 1196-1200.
Obi, S., Yamamoto, K., Shimizu, N., Kumagaya, S., Masumura, T., Sokabe, T., Asahara, T. and Ando, J. (2009). Fluid shear stress induces arterial differentiation of endothelial progenitor cells. *J. Appl. Physiol.* **106**, 203-211.
Oh, S. P., Seki, T., Goss, K. A., Imamura, T., Yi, Y., Donahoe, P. K., Li, L., Miyazono, K., ten Dijke, P., Kim, S. et al. (2000). Activin receptor-like kinase 1 modulates transforming growth factor-β1 signaling in the regulation of angiogenesis. *Proc. Natl. Acad. Sci. USA* **97**, 2626-2631.
Park, S. O., Lee, Y. J., Seki, T., Hong, K. H., Fliess, N., Jiang, Z., Park, A., Wu, X., Kaartinen, V., Roman, B. L. et al. (2008). ALK5- and TGFBR2-independent role of ALK1 in the pathogenesis of hereditary hemorrhagic telangiectasia type 2. *Blood* **111**, 633-642.
Park, S. O., Wankhede, M., Lee, Y. J., Choi, E. J., Fliess, N., Choe, S. W., Oh, S. H., Walter, G., Raizada, M. K., Sorg, B. S. et al. (2009). Real-time imaging of de novo arteriovenous malformation in a mouse model of hereditary hemorrhagic telangiectasia. *J. Clin. Invest.* **119**, 3487-3496.
Parmar, K. M., Larman, H. B., Dai, G., Zhang, Y., Wang, E. T., Moorthy, S. N., Kratz, J. R., Lin, Z., Jain, M. K., Gimbrone, M. A., Jr et al. (2006). Integration of flow-dependent endothelial phenotypes by Kruppel-like factor 2. *J. Clin. Invest.* **116**, 49-58.
Patrick, M. J., Chen, C. Y., Frakes, D. H., Dur, O. and Pekkan, K. (2010). Cellular-level near-wall unsteadiness of high-hematocrit erythrocyte flow using confocal PIV. *Experiments in Fluids* (in press) doi:10.1007/s00348-010-0943-8.
Quick, C. M., Hashimoto, T. and Young, W. L. (2001). Lack of flow regulation may explain the development of arteriovenous malformations. *Neurol. Res.* **23**, 641-644.
Rhoten, R. L., Comair, Y. G., Shedid, D., Chyatte, D. and Simonson, M. S. (1997). Specific repression of the preproendothelin-1 gene in intracranial arteriovenous malformations. *J. Neurosurg.* **86**, 101-108.
Roman, B. L., Pham, V. N., Lawson, N. D., Kulik, M., Childs, S., Lekven, A. C., Garrity, D. M., Moon, R. T., Fishman, M. C., Lechleider, R. J. et al. (2002). Disruption of acvrl1 increases endothelial cell number in zebrafish cranial vessels. *Development* **129**, 3009-3019.
Ross, S. and Hill, C. S. (2008). How the Smads regulate transcription. *Int. J. Biochem. Cell Biol.* **40**, 383-408.
Scharpfenecker, M., van Dinther, M., Liu, Z., van Bezooijen, R. L., Zhao, Q., Pukac, L., Lowik, C. W. and ten Dijke, P. (2007). BMP-9 signals via ALK1 and inhibits bFGF-induced endothelial cell proliferation and VEGF-stimulated angiogenesis. *J. Cell Sci.* **120**, 964-972.
Sehnert, A. J., Huq, A., Weinstein, B. M., Walker, C., Fishman, M. and Stainier, D. Y. (2002). Cardiac troponin T is essential in sarcomere assembly and cardiac contractility. *Nat. Genet.* **31**, 106-110.
Seki, T., Yun, J. and Oh, S. P. (2003). Arterial endothelium-specific activin receptor-like kinase 1 expression suggests its role in arterialization and vascular remodeling. *Circ. Res.* **93**, 682-689.
Sepich, D. S., Wegner, J., O'Shea, S. and Westerfield, M. (1998). An altered intron inhibits synthesis of the acetylcholine receptor alpha-subunit in the paralyzed zebrafish mutant nic1. *Genetics* **148**, 361-372.
Sharefkin, J. B., Diamond, S. L., Eskin, S. G., McIntire, L. V. and Dieffenbach, C. W. (1991). Fluid flow decreases preproendothelin mRNA levels and suppresses endothelin-1 peptide release in cultured human endothelial cells. *J. Vasc. Surg.* **14**, 1-9.
Siekmann, A. F., Standley, C., Fogarty, K. E., Wolfe, S. A. and Lawson, N. D. (2009). Chemokine signaling guides regional patterning of the first embryonic artery. *Genes Dev.* **23**, 2272-2277.
Sorensen, L. K., Brooke, B. S., Li, D. Y. and Urness, L. D. (2003). Loss of distinct arterial and venous boundaries in mice lacking endoglin, a vascular-specific TGFbeta coreceptor. *Dev. Biol.* **261**, 235-250.
Taber, L. A., Ng, S., Quesnel, A. M., Whatman, J. and Carmen, C. J. (2001). Investigating Murray's law in the chick embryo. *J. Biomech.* **34**, 121-124.
Toporsian, M., Gros, R., Kabir, M. G., Vera, S., Govindaraju, K., Eidelman, D. H., Husain, M. and Letarte, M. (2005). A role for endoglin in coupling eNOS activity and regulating vascular tone revealed in hereditary hemorrhagic telangiectasia. *Circ. Res.* **96**, 684-692.
Traver, D., Paw, B. H., Poss, K. D., Penberthy, W. T., Lin, S. and Zon, L. I. (2003). Transplantation and in vivo imaging of multilineage engraftment in zebrafish bloodless mutants. *Nat. Immunol.* **4**, 1238-1246.
Uchida, D., Onoue, T., Begum, N. M., Kuribayashi, N., Tomizuka, Y., Tamatani, T., Nagai, H. and Miyamoto, Y. (2009). Vesnarinone downregulates CXCR4 expression via upregulation of Kruppel-like factor 2 in oral cancer cells. *Mol. Cancer* **8**, 62.
Urness, L. D., Sorensen, L. K. and Li, D. Y. (2000). Arteriovenous malformations in mice lacking activin receptor-like kinase-1. *Nat. Genet.* **26**, 328-331.
Villefranc, J. A., Amigo, J. and Lawson, N. D. (2007). Gateway compatible vectors for analysis of gene function in the zebrafish. *Dev. Dyn.* **236**, 3077-3087.
Wang, D. L., Tang, C. C., Wung, B. S., Chen, H. H., Hung, M. S. and Wang, J. J. (1993). Cyclical strain increases endothelin-1 secretion and gene expression in human endothelial cells. *Biochem. Biophys. Res. Commun.* **195**, 1050-1056.
Wang, Y., Dur, O., Patrick, M. J., Tinney, J. P., Tobita, K., Keller, B. B. and Pekkan, K. (2009). Aortic arch morphogenesis and flow modeling in the chick embryo. *Ann. Biomed. Eng.* **37**, 1069-1081.
Westerfield, M. (1995). *The Zebrafish Book*. Eugene, OR: University of Oregon Press.
You, D., Waeckel, L., Ebrahimian, T. G., Blanc-Brude, O., Foubert, P., Barateau, V., Duriez, M., Lericousse-Roussanne, S., Vilar, J., Dejana, E. et al. (2006). Increase in vascular permeability and vasodilation are critical for proangiogenic effects of stem cell therapy. *Circulation* **114**, 328-338.